Time-resolved Fluorescence of the Single Tryptophan of *Bacillus stearothermophilus* Phosphofructokinase

Soon-Jong Kim, Fahmida N. Chowdhury, Wieslaw Stryjewski, Ezzat S. Younathan, Paul S. Russo, and Mary D. Barkley

Departments of Chemistry and Biochemistry, Louisiana State University, Baton Rouge, Louisiana 70803 USA

ABSTRACT   The fluorescence of the single tryptophan in *Bacillus stearothermophilus* phosphofructokinase was characterized by steady-state and time-resolved techniques. The enzyme is a tetramer of identical subunits, which undergo a concerted allosteric transition. Time-resolved emission spectral data were fitted to discrete and distributed lifetime models. The fluorescence decay is a double exponential with lifetimes of 1.6 and 4.4 ns and relative amplitudes of 40 and 60%. The emission spectra of both components are identical with maxima at 327 nm. The quantum yield is 0.31 ± 0.01. The shorter lifetime is independent of temperature; the longer lifetime has weak temperature dependence with activation energy of 1 kcal/mol. The fluorescence intensity and decay are the same in H_2O and D_2O solutions, indicating that the indole ring is not accessible to bulk aqueous solution. The fluorescence is not quenched significantly by iodide, but it is quenched by acrylamide with bimolecular rate constant of 5×10^8 M^{-1} s^{-1}. Static and dynamic light scattering measurements show that the enzyme is a tetramer in solution with hydrodynamic radius of 40 Å. Steady-state and time-resolved fluorescence anisotropies indicate that the tryptophan is immobile. The allosteric transition has little effect on the fluorescence properties. The fluorescence results are related to the x-ray structure.

INTRODUCTION

Phosphofructokinase (PFK) is a classical allosteric enzyme (1). It catalyzes the phosphorylation of D-fructose 6-phosphate (Fru6P) by ATP to form D-fructose 1,6-bisphosphate, a key regulatory step in glycolysis. The active enzyme from most sources is a tetramer, which undergoes a concerted two-state allosteric transition. The enzyme from *Bacillus stearothermophilus* (Bs-PFK) shows hyperbolic Michaelis-Menten kinetics with respect to both substrates, but cooperative kinetics in the presence of allosteric inhibitor phosphoenolpyruvate (PEP) (2). Unliganded Bs-PFK is in the active R state, which has high affinity for substrate, switching to the inactive T state with low affinity for substrate only in the presence of PEP.

Structures of Bs-PFK and the major PFK from *Escherichia coli* (Ec-PFK) have been determined by x-ray crystallography (3–5). These bacterial PFKs have four identical subunits of 34 kDa with 54% amino acid sequence homology (6–8). Their three-dimensional structures are very similar. The elongated subunits comprise two domains with an active site between them: the larger domain binds ATP substrate, and the smaller one binds Fru6P substrate. Both domains have a central β-sheet with layers of α-helices on either side. The enzyme is assembled as a dimer of dimers, so that each subunit contacts two other subunits. A large interface between monomers packed head-to-tail forms the dimer and the allosteric effector binding site. The single tryptophan is located at the large interface. A small interface between dimers packed head-to-tail forms the tetramer and the Fru6P substrate binding site.

Tryptophan fluorescence is potentially a powerful probe of the microenvironment in proteins because of the many nonradiative decay pathways available to the indole chromophore. Although indole itself has a monoexponential fluorescence decay, single tryptophan proteins almost invariably have complex decays (9). In some proteins the decay represents discrete lifetime components (10), whereas in others it is more likely a distribution of lifetimes (11). This complexity reports heterogeneity in the ground or excited state, arising from multiple conformational states of a dynamic protein structure. Variable proximity of excited indole to functional groups which may participate in nonradiative decay processes, such as proton transfer (12), electron transfer (13) or exchange, energy transfer (14), and solvent relaxation (15) or quenching (16), causes the lifetime heterogeneity. However, in most cases it has been difficult to pinpoint specific functional groups and nonradiative decay processes. A number of single tryptophan proteins have been studied with a view to relating the fluorescence decay to an x-ray or NMR structure. The goal is to develop a framework for interpreting the fluorescence from proteins over a wide range of circumstances including living cells. This paper contributes to that ongoing effort. Here we report time-resolved fluorescence measurements of Bs-PFK under several conditions: temperature, solute quenching, and inhibitor binding. Additional information is obtained from light scattering. Origins of the complex decay are discussed in light of the x-ray structure.

MATERIALS AND METHODS

Reagents

ATP, Fru6P, PEP, tryptophan, and *N*-acetyltryptophanamide were purchased from Sigma Chemical Co. (St. Louis, MO). Tris-(hydroxymethyl)-aminomethane (Tris) Ultra Pure and KI were purchased from Fisher Scientific (Pittsburgh, PA). Acrylamide (ultrapure) was purchased from ICN

Biomedicals Inc. (Irvine, CA). p-Terphenyl (99+%) was purchased from Aldrich Chemical Co. (Milwaukee, WI).

Bs-PFK was isolated from *E. coli* strain DF1020/pBR322/Bs-PFK (8) using the procedure of Kotlarz and Buc (17) as modified by French et al. (18). All purification steps were carried out at 0–4°C except the heat treatment. Homogeneity and isoelectric point of purified PFK were determined by gel electrophoresis on a PhastGel System (Pharmacia LKB Biotechnology Inc., Piscataway, NJ) using PhastGel gradient 10–15% sodium dodecyl sulfate gels and PhastGel IEF3-9 isoelectric focussing gels. The gels showed a single band when stained with Coomassie Brilliant Blue, indicating >95% purity. The isoelectric point of Bs-PFK is 5.5. Samples in deuterated buffer were prepared by lyophilizing a solution of Bs-PFK in 50 mM Tris, pH 8.0, and dissolving the pellet in D_2O. Bs-PFK is not inactivated by freezing or lyophilization.

The extinction coefficient of Bs-PFK was determined from absorbance measured on an Aviv model 118DS UV-VIS spectrophotometer. Protein concentration was determined using a Bio-Rad (Richmond, CA) protein assay kit. A value of $\epsilon_{278} = 16,600$ M^{-1} cm^{-1} was calculated based on a monomer molecular weight of 34,122 (8). Bs-PFK solutions are prepared in 50 mM Tris, pH 8.0, unless otherwise noted; molar concentrations are expressed on a monomer basis.

Steady-state fluorescence

Fluorescence was measured on a SLM model 8000 photon counting spectrofluorometer with single excitation (4-nm bandpass) and emission (8-nm bandpass) monochromators. The excitation wavelength was 296 nm to avoid excitation of tyrosine and phenylalanine. Anisotropic effects were eliminated by using magic angle polarizers, which were set at 55° on the excitation side and 0° on the emission side to avoid the Wood's anomaly of the emission grating. Sample absorbance was <0.1 at 296 nm with 0.4-cm path length. Fluorescence emission was measured in the ratio mode, and background fluorescence from a solvent blank was subtracted. Emission spectra were corrected for the wavelength dependence of the instrument response using correction factors determined with a standard lamp from Optronics Laboratories Inc. (Orlando, FL). Temperature was controlled by a circulating water bath.

Fluorescence quantum yields were measured by comparison to tryptophan (recrystallized four times from 70% ethanol) in water. Sample quantum yields were calculated using a value of 0.14 for tryptophan at 25°C (19). The temperature dependence of the quantum yield was analyzed assuming a single temperature-dependent deactivation process (20).

$$\Phi^{-1} = k_o/k_r + (A/k_r) \exp(-E^*/RT) \tag{1}$$

Φ is the quantum yield at absolute temperature T, k_r is the radiative rate, k_o is the total temperature-independent rate ($k_o = k_r + k_{nr}$, where k_{nr} is the temperature-independent nonradiative rate), A is the frequency factor, E^* is the activation energy, and R is the gas constant. The value of k_r was determined from quantum yield and lifetime data: $k_r = \Phi/\bar{\tau}$, where $\bar{\tau} = \Sigma_i \alpha_i \tau_i/\Sigma_i \alpha_i$. The Arrhenius parameters A and E^* were estimated from a least squares fit of $\ln[\Phi^{-1} - k_o/k_r]$ vs. $1/RT$ using a literature value of k_o (16, 21).

Solute quenching experiments were carried out using stock solutions of 1, 2, and 8 M acrylamide and 1 M KI in water. Ionic strength was kept constant in iodide quenching experiments by diluting Bs-PFK into 50 mM Tris, pH 8.0, containing 1 M KCl. Intensities were acquired at 340-nm emission wavelength for five 10-s time intervals. Values were averaged and fit to the Stern-Volmer equation by least squares.

$$I_0/I = 1 + K_{SV}[Q] \tag{2}$$

I_o and I are fluorescence intensities in the absence and presence of quencher Q. $K_{SV} = k_q\tau_0$ is the Stern-Volmer constant, k_q is the quenching rate constant, and τ_0 is the fluorescence lifetime in the absence of quencher.

Fluorescence emission anisotropy was measured at 340-nm emission wavelength. Each data point was acquired for five 10-s time intervals, and the values were averaged. The anisotropy $\langle r \rangle$ was calculated from

$$\langle r \rangle = (I_{VV} - GI_{VH})/(I_{VV} + 2GI_{VH}) \tag{3}$$

where the first and second subscripts refer to the orientation of the excitation and emission polarizers, respectively (V = 0°; H = 90°), and $G = I_{HV}/I_{HH}$ is an instrumental correction factor.

Time-resolved fluorescence

Fluorescence decays were measured by time-correlated single photon counting on a Photochemical Research Associates instrument with a picosecond rhodamine dye laser excitation source as described before (16). Decay curves were acquired in 512 channels of 54 or 108 ps/channel to about 3–3.5 $\times$ 10^4 counts in the peak. The reference fluorophore was p-terphenyl in 75% ethanol, 0.8 M KI (containing a trace of thiosulfate to retard I_3^- formation). Reference lifetimes measured with N-acetyltryptophanamide in 50 mM Tris, pH 8.0, as monoexponential standard ranged from 0.23 ns at 15°C to 0.15 ns at 50°C.

Decay data were analyzed by the Beechem global program (22), which was modified for reference deconvolution (23). In addition to discrete sums of exponentials and continuous distributions, this program does one-step analysis of temperature, quenching, and anisotropy data. Goodness of fit is judged by reduced chi squared χ_r^2 value, weighted residuals, and autocorrelation function of the residuals.

Lifetimes

The discrete analysis assumes a multiexponential decay model

$$I(t) = \Sigma_i \alpha_i \exp(-t/\tau_i) \tag{4}$$

with amplitudes α_i and lifetimes τ_i. Decay-associated emission spectra are derived by combining time-resolved and steady-state data

$$I_i(\lambda) = I(\lambda)\alpha_i(\lambda)\tau_i/\Sigma_i \alpha_i(\lambda)\tau_i \tag{5}$$

where $I(\lambda)$ is the steady-state intensity and $\alpha_i(\lambda)$ is the amplitude of component i at wavelength λ.

The distribution analysis used a continuous Gaussian amplitude profile of the lifetimes

$$I(t) = \Sigma_i \int \alpha(\tau_i) \exp(-t/\tau_i) \, d\tau_i \tag{6}$$

where the fitting parameters are the lifetime centers τ_c and the standard deviations σ in the Gaussian probability density function as follows.

$$\alpha(\tau) = (1/2\pi\sigma)^{1/2} \exp[-(\tau - \tau_c)^2/2\sigma^2] \tag{7}$$

Lifetime centers and standard deviations are linked in global analyses of time-resolved emission spectral data. To test whether the width of the distribution varies with emission wavelength, some analyses were performed with the standard deviations unlinked.

Arrhenius parameters were determined from temperature data by two methods: 1) single curve discrete analysis of decay curves at each temperature followed by least squares fit of lifetimes to the equation

$$\tau^{-1} = k_o + A \exp(-E^*/RT) \tag{8}$$

and 2) global analysis of the data at different temperatures directly in terms of k_o, A, and E^*:

$$I(t) = \Sigma_i \alpha_i \exp\{-t[k_{oi} + A_i \exp(-E_i^*/RT)]\}. \tag{9}$$

The Arrhenius parameters for component i, k_{oi}, A_i, and E_i^*, are linked for the entire temperature-dependent data set, leaving only the amplitudes free.

Solute-quenching data were also analyzed by two methods: 1) single curve discrete analysis of decay curves at each quencher concentration followed by least squares fit of lifetimes to the Stern-Volmer equation

$$1/\tau = 1/\tau_0 + k_q[Q] \tag{10}$$

and 2) global analysis of the data at different quencher concentrations directly in terms of τ_o and k_q, linking them for the entire quenching data set.

$$I(t) = \Sigma_i \alpha_i \exp[-t(1/\tau_{oi} + k_{qi}[Q])] \qquad (11)$$

Anisotropy decay

The polarized decays $I_{VV}(t)$ and $I_{VH}(t)$ were acquired contemporaneously with a reference decay in a four-cell sample holder. The $I_{VV}(t)$ and $I_{VH}(t)$ curves were collected for equal times in 512 channels of 108 ps/channel to about 3×10^4 peak counts in the $I_{VH}(t)$ curve. The polarized decays were fit simultaneously to

$$I_{VV}(t) = (1/3)I(t)[1 + 2\,r(t)] \qquad (12)$$

and

$$I_{VH}(t) = (1/3)GI(t)[1 - r(t)] \qquad (13)$$

where $I(t)$ is the intensity decay given by Eq. 4 and $r(t)$ is the anisotropy decay

$$r(t) = \Sigma_i\,\beta_i\exp(-t/\phi_i) \qquad (14)$$

with preexponentials β_i and rotational correlation times ϕ_i. The initial anisotropy $r(0) = \Sigma_i\beta_i$. The preexponentials and rotational correlation times are linked in the global analysis. The G factor was computed separately from

$$G = (\langle I_{VV}(t)\rangle/\langle I_{VH}(t)\rangle)(1 - \langle r\rangle)/(1 + 2\langle r\rangle) \qquad (15)$$

where $\langle I_{VV}(t)\rangle$ and $\langle I_{VH}(t)\rangle$ stand for the total counts in the respective curves and $\langle r\rangle$ is the steady-state anisotropy determined according to Eq. 3. The value of G was fixed in the global analysis. Instead of dividing the recovered α_i values of the $I_{VH}(t)$ curve by G as indicated in Eq. 13, the reference decay for the $I_{VH}(t)$ curve was multiplied by G.

Light scattering

A Lexel model 95 argon ion laser with maximum output of 1.4 watts at 514.5 nm was used as light source. The locally built apparatus has undergone only minor modifications since last described (24). The temperature was controlled at $25.00 \pm 0.05°C$ by a circulating water bath. Scattering cells were 12-mm OD silanated cells. Each cell was individually tested for cleanliness by filling it with clean water gravity fed (about 1-m pressure head) through a Gelman 0.2 μm cartridge filter. The flow rate of about 400 ml/min is sufficiently slow to prevent filter shedding. The water appeared completely free of dust as observed with a focussed laser beam traversing the water at 100 $\times$ magnification. Cells were checked after cleaning by observing the laser beam at 30° scattering angle. The cleaning process was repeated until less than one "dust-event"/30 s occurred. The scattering volume during measurement is much smaller than during cell testing, so dust is extremely unlikely during measurement. About 0.03–0.2 mg/ml Bs-PFK solutions were prepared in filtered buffer and transferred to cells via 0.2 μm Sargent-Welch Anotop prefabricated inorganic membrane filters. Very low protein binding on these filters was confirmed by UV and fluorescence measurements. Performance of the filters was variable, so the ability of each to deliver clean filtrate was judged by the laser observation test before use. Sample cells were capped with Teflon tape, and light scattering measurements were carried out immediately. Occasionally, it was necessary to centrifuge the samples directly in the cells at 9,000 g for 1 h.

Static light scattering was measured at 45° scattering angle. Average intensity was measured by repeated photon counting trials. Each measurement was accepted only after reproducibility was established. High intensity trials were eliminated from consideration as a dust-discriminating tool. The data were converted to Rayleigh factor using toluene as a reference standard. The Rayleigh factor for toluene as a reference at 90° scattering angle is $R = 1.402 \times 10^{-5}$ cm^{-1} at 632.8 nm (25). The value at 514.5 nm was calculated from $R_{514.5} = R_{632.8} (632.8/514.5)^4$. Assuming scattering of ver-

tically polarized incident light from a small, optically isotropic particle,

$$Kc/R_\theta = M_w^{-1} + 2A_2c \qquad (16)$$

where K is an optical constant containing the specific refractive index increment dn/dc, c is concentration in g/ml, R_θ is the Rayleigh ratio, M_w is weight-average molecular weight, and A_2 is the virial coefficient. M_w was obtained from the inverse intercept of the plot of Kc/R_θ vs. c by linear regression.

Dynamic light scattering was measured at 60° scattering angle. Each autocorrelation function (26) was obtained as the sum of several "short" runs, sometimes collected under manual supervision while observing a rate meter to guard against dust. Selected short runs were summed after testing each for consistency of intensity, average decay rate, degree of nonexponentiality, optical coherence, and agreement of computed and measured baselines (27). The summed baseline was typically 10^6–10^7. The data were fit using the method of cumulants (28). They were also fit by nonlinear least squares to a single exponential with a floating baseline. The hydrodynamic radius R_h was calculated from the Stokes-Einstein equation

$$D = kT/6\pi\eta_0 R_h \qquad (17)$$

where D is the translational diffusion coefficient, k is the Boltzmann constant, and η_0 is solvent viscosity. The uncertainty in hydrodynamic radius was obtained from the difference between cumulants and nonlinear least squares analyses.

RESULTS

Single tryptophan has two decay components in similar environments

The fluorescence decay of Bs-PFK was measured at 5-nm intervals from 315- to 360-nm emission wavelength at 25°C. The time-resolved emission spectral data were deconvolved using both discrete and distributed decay models. Table 1 summarizes the results of global analyses with the lifetimes linked. The global fit to a single exponential function was unsatisfactory with a χ_r^2 value of 25. Correcting for scattered light did not improve the fit. The double exponential fit gave an acceptable $\chi_r^2 = 1.50$. Inclusion of a term for scattered light made little difference in the decay parameters but improved χ_r^2 slightly to 1.45. The weighted residuals and autocorrelation function did not reveal significant nonrandomness (Fig. 1 a). A triple exponential fit further lowered χ_r^2 to 1.34. However, the recovered values of decay parameters for

TABLE 1   Fluorescence decay parameters, 25°C

Model	Amplitude α_i or area	Lifetime τ_i or τ_c	Standard deviation σ	χ_r^2
		ns	ns	
Discrete				
Single exponential	1.00	3.51		24.9
Double exponential	0.41 ± 0.03	1.64		1.45
	0.59 ± 0.01	4.43		
+0.1 M PEP	0.40	1.64		1.51
	0.60	4.43		
Distribution				
Unimodal Gaussian	1.00	3.35	1.59	1.91
Bimodal Gaussian	0.33	1.62	0.48	1.24
	0.67	4.31	0.67	

[Bs-PFK] = 6×10^{-6} M, pH 8.0. Global analysis of data acquired at 296-nm excitation, 315–360-nm emission wavelength (5-nm intervals). Experiments were performed in the presence of PEP at 340-nm emission wavelength. Results of analyses with scatter correction.
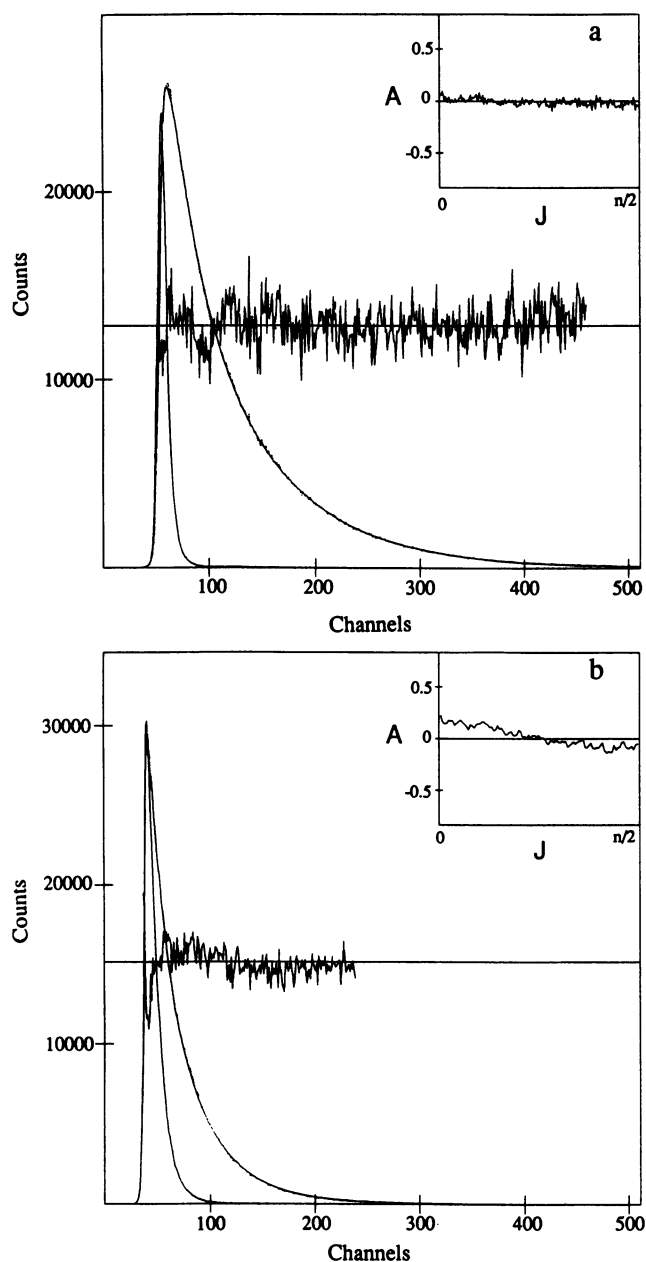
FIGURE 1   Time-resolved fluorescence. Left solid line is reference decay; dotted line is sample decay; data are from experiments at 296-nm excitation, 340-nm emission wavelength, 25°C. Weighted percent residuals and autocorrelation function of the residuals (*inset*) are also shown. (*a*) Intensity decay, 54 ps/channel. Smooth curve is best fit in global analysis of time-resolved emission spectral data: $\alpha_1 = 0.42$, $\tau_1 = 1.64$ ns, $\alpha_2 = 0.58$, $\tau_2 = 4.43$ ns; partial $\chi_r^2 = 1.36$. 0.2% scatter. (*b*) Horizontally polarized anisotropy decay, 108 ps/channel. Smooth curve is best fit in global analysis of polarized decays and magic angle decay, $G = 0.552$: $\alpha_1 = 0.38$, $\tau_1 = 1.79$ ns, $\alpha_2 = 0.62$, $\tau_2 = 4.52$ ns, $\beta = 0.191$, $\phi = 42.6$ ns; partial $\chi_r^2 = 1.46$. 5.6% scatter. The nonrandom autocorrelation function is probably due to error in G.

three exponential models were sensitive to initial guesses. Also, we were unable to resolve three exponentials in the temperature, quenching, and anisotropy data presented later. The data were also analyzed by unimodal and bimodal Gaus-

sian distribution models with and without correction for scattered light. Among these analyses, the lowest χ_r^2 value of 1.24 was obtained for the bimodal Gaussian distribution with scatter correction (Fig. 2). The lifetime centers and relative heights of the bimodal Gaussian distribution coincide with the discrete lifetimes and amplitudes of the biexponential fit. The apparent width of the α vs. τ profile does not automatically mean a true distribution. Such widths were also obtained from distribution analyses of data simulated for discrete models. Moreover, the temperature, quenching, and anisotropy data did not support a bimodal distribution model. In distinguishing the discrete biexponential and unimodal Gaussian distribution models, we note that increasing the number of components in the discrete model should lead to progressively better fits of data from a true distribution (Q. Chen, F. N. Chowdhury, K. Maskos, and M. D. Barkley, manuscript in preparation). This trend was not seen in the Bs-PFK lifetime data. The triple exponential fit showed little improvement over the double exponential fit and attempts to include more components resulted in obvious redundancy. Therefore, a discrete biexponential model best describes the fluorescence decay of the single tryptophan in Bs-PFK, at least at the statistical precision of the data.

Fig. 3 shows the steady-state emission spectrum of Bs-PFK together with the decay-associated spectra of the two components constructed according to Eq. 5. The relative amplitudes of the two components are independent of emission wavelength (Table 1), indicating that their emission spectra have the same shape. This argues that the two decay components originate from similar ground- and excited-state environments. The 1.6-ns component contributes 20% and the 4.4-ns component contributes 80% of the total fluorescence intensity.
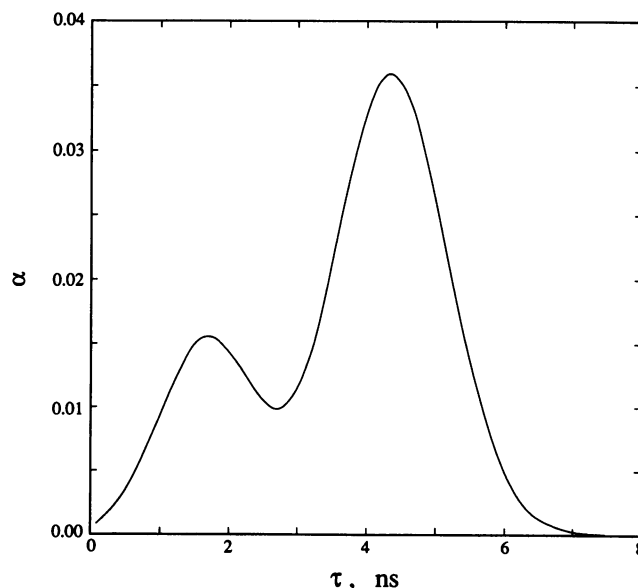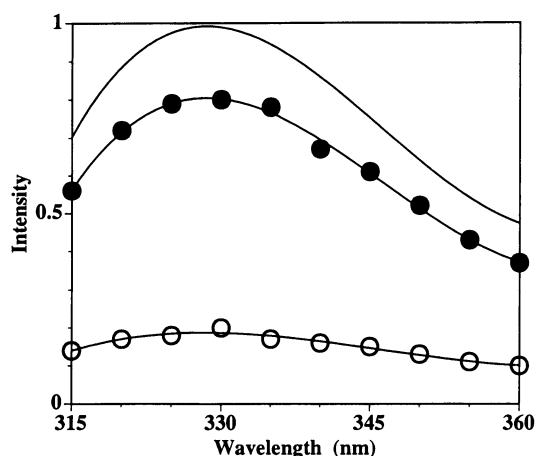

FIGURE 2   Bimodal lifetime distribution.

FIGURE 3   Decay-associated emission spectra of (○) $\tau_1 = 1.6$-ns and (●) $\tau_2 = 4.4$-ns components of Bs-PFK. Top curve is steady-state emission spectrum. Excitation wavelength was 296 nm, at 25°C.

Fluorescence is weakly temperature-dependent

The fluorescence quantum yield and lifetime of Bs-PFK were measured at 5° intervals between 15 and 50°C. The enzyme is stable up to 70°C. Table 2 presents the results obtained from single curve analyses of the decay curves acquired at each temperature. The longer lifetime decreases slightly with increasing temperature, but the shorter component shows almost no temperature dependence over this range. The relative amplitudes are independent of temperature. The radiative rate calculated from quantum yield and lifetime data, $k_r = 8.0 \pm 0.2 \times 10^7$ s^{-1}, is independent of temperature. This is close to the values reported for N-acetyltryptophanamide in dioxane (29) and the partially buried tryptophan in RNase T1 (30). It is somewhat higher than usual for aqueous tryptophan derivatives (20, 31) and other single tryptophan proteins (32, 33).

We assume that a single temperature-dependent nonradiative process accounts for the temperature dependence of Bs-PFK fluorescence. Arrhenius parameters were extracted from quantum yield data using a temperature-independent rate $k_o = 1 \times 10^8$ s^{-1} (34) in Eq. 1. Table 3 shows the results, together with results obtained from various analyses of temperature-dependent lifetime data. The plot of $\ln[\Phi^{-1} - $

TABLE 3   Arrhenius parameters

	k_o	A	E
Quantum yield	s^{-1}	s^{-1}	kcal/mol
Linear fit	1×10^8	2.6×10^9	1.4
Lifetime, τ_1			
Linear fit	1×10^8	2.8×10^9	1.11
Nonlinear fit	5.7×10^8	6.5×10^{15}	11
Global analysis	5.5×10^8		
Lifetime, τ_2			
Linear fit	1×10^8	7.5×10^8	1.05
Nonlinear fit	1.6×10^8	1.7×10^{10}	1.9
Global analysis	1.1×10^8	4.6×10^8	0.81

$k_o/k_r]$ vs. $(RT)^{-1}$ is linear (Fig. 4 a), giving values for the frequency factor $A = 2.6 \times 10^9$ s^{-1} and activation energy $E^* = 1.4$ kcal/mol. Nonlinear fitting of quantum yield data directly to Eq. 1 turned out to be quite sensitive to initial guesses because of the weak temperature dependence relative to the precision of quantum yield data.

The lifetime data in Table 2 were fitted to both linear and nonlinear forms of the Arrhenius equation. Fig. 4 b shows the nonlinear fit to Eq. 8. The fluctuations in the shorter lifetime result in poor fits for both linear and nonlinear cases. The
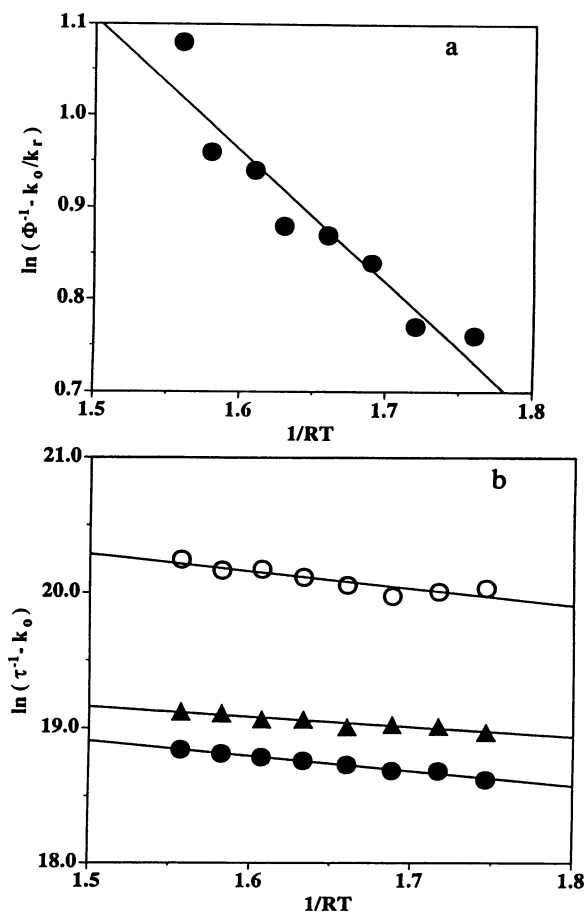

FIGURE 4   Arrhenius plots assuming $k_o = 1 \times 10^8$ s^{-1}. (a) Quantum yield, 296-nm excitation wavelength. (b) Lifetime: (○) τ_1, (●) τ_2, and (▲) $\bar{\tau}$; data from Table 2.

TABLE 2   Temperature dependence of fluorescence lifetimes

Temp	α_1	τ_1	τ_2	χ_r^2
°C		ns	ns	
15	0.40	1.66	4.51	1.87
20	0.40	1.69	4.34	1.60
25	0.38	1.74	4.34	1.51
30	0.45	1.63	4.23	1.57
35	0.45	1.55	4.16	1.46
40	0.44	1.48	4.10	1.55
45	0.45	1.48	4.03	1.53
50	0.44	1.39	3.96	1.62

[Bs-PFK] = 6×10^{-6} M, pH 8.0. Single curve analysis of data acquired at 296-nm excitation, 340-nm emission wavelength, with scatter correction.

frequency factors A and activation energies E^* obtained for the longer lifetime are in reasonable agreement with the values from quantum yield data (Table 3). The temperature-independent rate k_{o1} estimated from the nonlinear fit of the shorter lifetime ($1/k_{o1} = 1.76$ ns) suggests that there is almost no temperature dependence of this lifetime ($\tau_1 = 1.74$ ns at 25°C). Finally, the decay curves were analyzed directly in terms of the Arrhenius parameters, bypassing the recovery of lifetimes. The Arrhenius parameters k_{oi}, A_i, and E_i^* of the two components were linked at different temperatures in the global analysis. The robustness of each result was tested by repeating the analysis with different initial guesses. The best global χ_r^2 obtained was 1.64, where we assumed that the shorter lifetime ($1/k_{o1} = 1.82$ ns) did not depend on temperature. This model gave k_{o2}, A_2, and E_2^* values of 1.1×10^8 s^{-1}, 4.6×10^8 s^{-1}, and 0.81 kcal/mol, respectively, for the longer lifetime. Attempts to include two temperature-dependent terms in Eq. 9 resulted in very low frequency factors and a nearly flat lifetime vs. temperature function ($1/k_{o1} = 2.0$ ns) for the short component. Thus we concluded that the shorter lifetime is essentially independent of temperature, whereas the longer lifetime has a slight temperature dependence with an activation energy E^* of about 1 kcal/mol.

Tryptophan is inaccessible to solvent

The fluorescence quantum yield and lifetime of indole derivatives increase in D$_2$O compared to H$_2$O (35). A solvent isotope effect on tryptophan fluorescence in proteins signifies exposure of the tryptophan environment to aqueous solvent. The intensity and lifetime of Bs-PFK fluorescence were measured 2, 6, and 30 days after dissolving the enzyme in deuterated buffer. There is no deuterium isotope effect on the fluorescence (Table 4), indicating that the tryptophan at the monomer subunit interface is not accessible to bulk solvent.

The accessibility of the tryptophan to small solute molecules was probed by collisional quenching experiments using acrylamide and iodide. Both are efficient quenchers of indole fluorescence (36). Fig. 5 shows Stern-Volmer plots of the intensity and lifetime quenching data. Bs-PFK fluorescence is quenched by acrylamide, but not significantly quenched by iodide (Fig. 5 a). The apparent bimolecular quenching rate k_q(app) was estimated from the steady-state Stern-Volmer constant

$$K_{SV} = k_q(\text{app})\langle \tau_{io} \rangle \qquad (18)$$

TABLE 4 Fluorescence in H$_2$O and D$_2$O, 25°C

D$_2$O	I_{D_2O}/I_{H_2O}	α_1	τ_1	τ_2	$\bar{\tau}$	χ_r^2
days			ns	ns	ns	
0	1.0	0.39	1.63	4.42	3.33	1.51
2	1.0	0.43	1.50	4.60	3.27	1.45
6	1.0	0.45	1.81	4.61	3.35	1.27
30	1.0	0.46	1.58	4.64	3.23	1.48

[Bs-PFK] = 6×10^{-6} M, pH(D) = 8.0. Single curve analysis of data acquired at 296-nm excitation, 340-nm emission wavelength, with scatter correction.
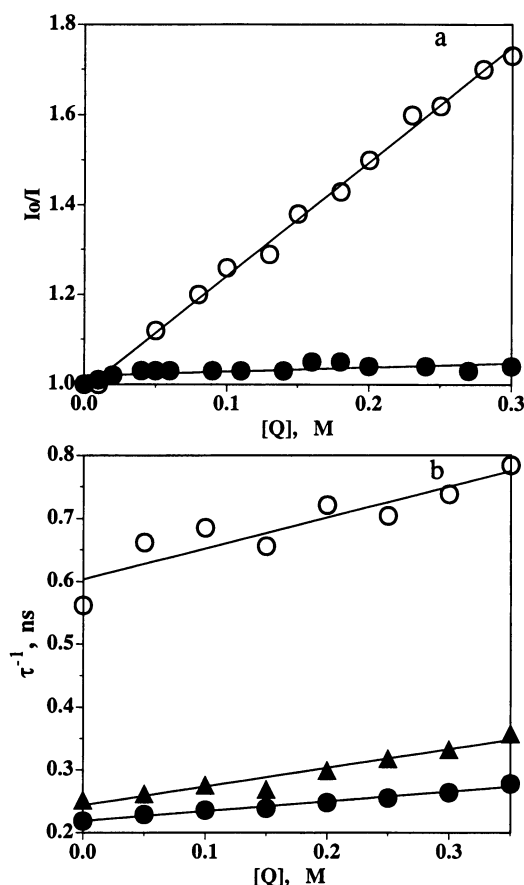
FIGURE 5 Stern-Volmer plots. (a) Steady-state intensity: (O) acrylamide and (●) iodide. (b) Lifetime: (O) τ_1, (●) τ_2, and (▲) $\langle \tau \rangle$. Excitation wavelength was 296 nm, and emission wavelength was 340 nm. Temperature was 25°C.

where $\langle \tau_o \rangle = \Sigma_i \alpha_i \tau_{io}^2 / \Sigma_i \alpha_i \tau_{io}$ is the mean lifetime. The value of k_q(app) = 5.4×10^8 M^{-1} s^{-1} for acrylamide is at least 10 times faster than for iodide, though below the diffusion limit for fully exposed indoles (Table 5). Moreover, the two lifetime components are quenched by acrylamide at different rates (Fig. 5 b). The individual bimolecular quenching rates k_{qi} obtained from a two-step analysis of the time-resolved data agreed quite well with those recovered by global analysis directly in terms of the Stern-Volmer parameters (Table 5). The values of τ_{oi} and k_{qi} at different acrylamide concentrations were linked in the global analysis, which gave a global χ_r^2 of 1.92 and remarkably robust results. The shorter lifetime component is quenched almost four times faster than the longer lifetime component. The bimolecular quenching rate for the mean lifetime is 3.3×10^8 M^{-1} s^{-1}, which is reasonably close to the apparent value from steady-state quenching experiments. This argues against static quenching of Bs-PFK fluorescence by acrylamide.

Bs-PFK is a tetramer in solution

The molecular weight of Bs-PFK was measured by static light scattering at pH 6.0 and 8.0. The experiments were done

TABLE 5 Stern-Volmer parameters, 25°C

		Unquenched lifetime			Bimolecular quenching rate $\times$ 10^{-8} M^{-1} s^{-1}		
	Quencher	$\langle \tau_o \rangle$	τ_{o1}	τ_{o2}	$k_q(app)$	k_{q1}	k_{q2}
		ns			ns		
Intensity	Acrylamide	4.01			5.4 $\pm$ 0.8		
+0.1 M PEP		3.87			6.3 $\pm$ 0.5		
	Iodide	4.01			0.5		
+0.1 M PEP		3.87			0.2		
Lifetime	Acrylamide						
Linear fit			1.65	4.59	3.3	4.5	1.4
Global			1.63	4.52		4.0	1.4

[Bs-PFK] = 6 $\times$ 10^{-6} M, pH 8.0; 296-nm excitation, 340-nm emission wavelength.

within the concentration range of the fluorescence measurements. As the molecules are quite small compared to the laser wavelength, it was impossible to measure static radii of gyration. On the positive side, molecular weights could be determined reliably by scattering measurements at a single scattering angle. Fig. 6 shows intensity data plotted according to Eq. 16, assuming a reasonable value of dn/dc = 0.195 ml/g for proteins (37). The scatter in the data reflects the very low concentrations and small excess light scattering compared to solvent. (Protein scattering was only a few percent above solvent at lower concentrations.) However, the intercepts can be estimated to within about 15%, yielding molecular masses of 122 and 116 kDa at pH 6.0 and 8.0, respectively. These values are within experimental error of the tetramer molecular mass of 136 kDa.

The translational diffusion coefficient of Bs-PFK at 25°C was determined by dynamic light scattering from pH 6.0 to 9.0 at a protein concentration of 0.2 mg/ml (6 $\times$ 10^{-6} M). Due to the low concentrations, apparent optical coherence was

reduced compared to strongly scattering solutions (38). Nevertheless, acceptable correlation functions could be acquired within a reasonable time, and the average decay rate was readily determined (Fig. 7). The hydrodynamic radius R_h was calculated using the z average diffusion coefficient D_z in Eq. 17. As seen in Table 6, the hydrodynamic radius of Bs-PFK hovers around 40 Å. The isoelectric point of the enzyme is 5.5, so the slight decrease and greater uncertainty in hydrodynamic radius at pH 6.5 cannot be attributed to anomalous behavior at the isoelectric point. Paradies et al. (39) measured a value of 34.4 Å for the radius of gyration R_g of Ec-PFK by small angle x-ray scattering. Their reported value of the Stokes' radius R_h was apparently derived for a spherical model by multiplying R_g by $\sqrt{5/3}$ to give 44.4 Å. (The number cited in Ref. 39 is 44.0 Å in the abstract and 44.3 Å in Table 1.) However, the value of R_h = 53.4 Å computed from the diffusion coefficient reported by Paradies et al. (39) is significantly larger than we obtain. A spherical, unhydrated protein of mass 136 kDa and partial specific volume 0.745
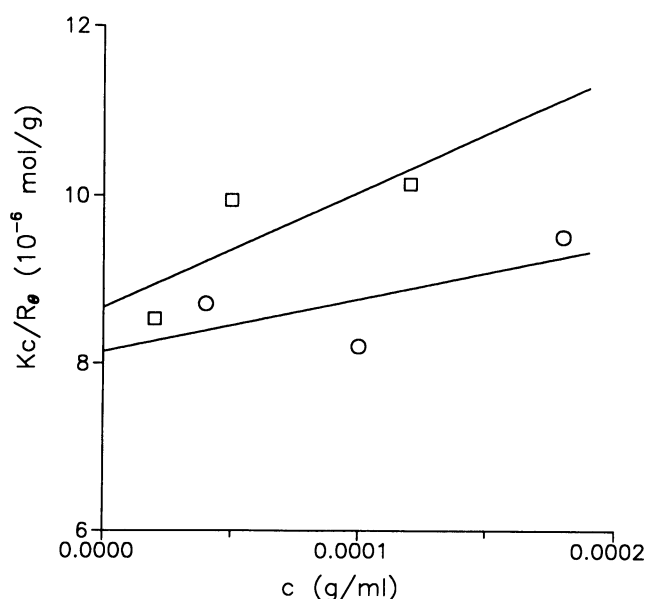
FIGURE 6 Static light scattering as a function of Bs-PFK concentration in (O) 0.01 M acetate, pH 6.0, and (■) 0.01 M Tris, pH 8.0. 25°C, θ = 45°. M_w^{-1} is the intercept at c = 0.
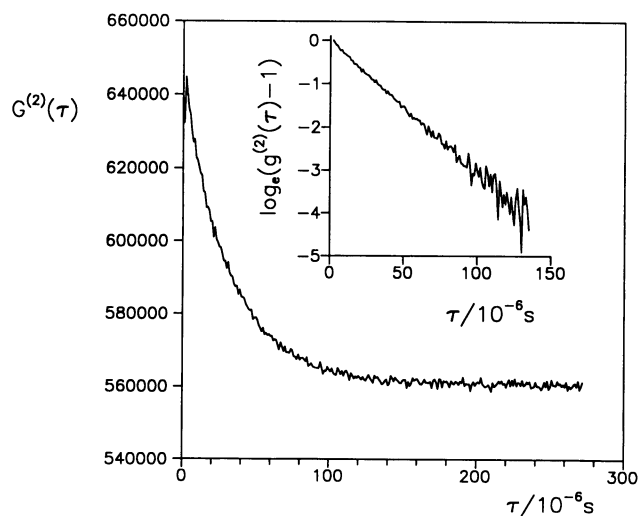
FIGURE 7 Light scattering second order intensity autocorrelation function $G^{(2)}(\tau)$. θ = 60°, 0.2 mg/ml Bs-PFK in 0.01 M Tris, pH 8.5, 25°C; τ is the lag time. Inset is semilog representation of the normalized, baseline-subtracted, second order correlation function, $g^{(2)}(\tau) - 1$. Lack of curvature indicates that the sample is monodisperse.

TABLE 6 Light scattering quantum yield, and emission anisotropy data, 25°C

| pH	Molecular mass	R_h	F	$\langle r \rangle$
	kDa	Å		
5.5		39 ± 1	0.33 ± 0.02	0.174
6.0	122		0.33 ± 0.02	0.175
6.5		34 ± 4	0.32 ± 0.02	0.173
7.0			0.31 ± 0.03	0.174
7.5		41 ± 1	0.30 ± 0.02	0.174
8.0	116		0.30 ± 0.02	0.177
+0.1 M PEP			0.28	0.170
8.5		39 ± 2	0.31 ± 0.02	0.174

0.01 M buffer: acetate, pH 5.5–6.0; 1,3-bis[tris(hydroxymethyl)-methylamine]propane, pH 6.5–7.0; Tris, pH 7.5–8.5.

TABLE 7 Anisotropy decay parameters, 25°C

Global analysis	Lifetimes		β	ϕ	χ_r^2
	τ_1	τ_2			
	ns			ns	
Polarized decays	2.09	4.67	0.19	41.9	1.33
Polarized decays, magic angle decay	1.79	4.52	0.19	42.1	1.38

[Bs-PFK] = 6 × 10⁻⁶ M, pH 8.0; 296-nm excitation, 340-nm emission wavelength.

ml/g has a radius of 34.3 Å. Similarly, each subunit of mass 34 kDa has an equivalent radius b = 21.6 Å. According to simple Kirkwood-Risemann theory, the hydrodynamic radius of a tetrahedral arrangement of four such spheres is $8b/5$ = 34.5 Å (40). The measured hydrodynamic radius of about 40 Å exceeds that of a single sphere of equivalent mass by a factor of 1.15. If the protein is not hydrated, this factor can be accounted for by a prolate or oblate ellipsoid of axial ratio of about 3, which is somewhat larger than the axial ratio of 1.3–1.5 estimated from the x-ray structure (5). Therefore, some hydration of the protein is probably indicated.

Tryptophan is immobilized in Bs-PFK

The Stokes shift of the indole chromophore is highly sensitive to solvent polarity, moving about 50 nm to the red from hexane to water (41). The emission maxima of tryptophan residues in proteins range from 308 to 350 nm (9). Bs-PFK fluorescence has a maximum at 327 nm, suggesting a relatively nonpolar environment. At 25°C, the fluorescence quantum yield is 0.31 ± 0.01 and the steady-state emission anisotropy at 296 nm excitation is 0.175 ± 0.003. The emission maximum, quantum yield, and anisotropy are constant from pH 6 to 9 (Table 6). The steady-state anisotropy at 25°C is within the range 0.167–0.194 for frozen solutions of single tryptophan peptides and proteins excited at 295 nm (42), but below the limiting value of 0.28 for tryptophan at this excitation wavelength (43).

The time-resolved emission anisotropy of Bs-PFK was measured at 25°C. The vertically and horizontally polarized decays were deconvolved simultaneously with all of the decay parameters linked (Table 7). The fit assuming a monoexponential anisotropy decay gave a global χ_r^2 of 1.33 with rotational correlation time ϕ = 41 ns and preexponential β = 0.19 (Fig. 1 b). However, the shorter lifetime τ_1 = 2.1 ns is somewhat larger than the value of 1.63 ns recovered from magic angle experiments (Table 1). Attempts to resolve a biexponential anisotropy decay failed. The analysis either returned two 41-ns components or gave a fast ϕ with very small β (0.001) or very slow ϕ (130 ns) with negative β for the second component. Including a magic angle decay in the global analysis yields a 1.79-ns lifetime for the short com-

ponent with almost no change in the anisotropy decay parameters. We note that the confidence interval for the correlation time is very wide. Varying ϕ between 30 and 60 ns (5-ns intervals), while keeping the other parameters fixed, increased the χ_r^2 value 5% at most. A rotational correlation time 10 times the excited-state lifetime is poorly determined. The hydrodynamic volume V_h was calculated from the Stokes-Einstein equation as follows.

$$\phi = V_h \eta_o / kT \qquad (19)$$

The value of 1.9 × 10⁻¹⁹ cm³ is slightly larger than the estimated volume of 1.7 × 10⁻¹⁹ cm³ for a sphere equivalent to Bs-PFK. The initial anisotropy $r(0)$ = 0.19 falls in the range of values of 0.18–0.26 reported for RNase T1 at 295-nm excitation wavelength (30, 44). The anisotropy decay of the single tryptophan of RNase T1 is also single exponential. The relatively high values of the steady-state and initial anisotropies as well as the single long rotational correlation time argue that the indole ring is firmly anchored in the monomer subunit interface.

Tryptophan environment is similar in R and T states

Bs-PFK switches from the active R state to the inactive T state in the presence of the allosteric inhibitor PEP (5). Fluorescence measurements were made on enzyme-ligand complexes at 25°C. No changes in fluorescence were observed in the presence of Fru6P and ATP substrates, consistent with an R-state conformation for unliganded Bs-PFK. In the presence of PEP the fluorescence emission maximum shifts about 2 nm to the red, and the quantum yield drops about 10% compared to enzyme alone (Table 6). These changes, albeit small, are reproducible and reversible by addition of Fru6P substrate. The fluorescence decay of the inhibitor complex has two components with the same amplitudes and lifetimes as the free enzyme (Table 1). The emission anisotropy and quenching rates were not affected by PEP (Tables 5, 6).

DISCUSSION

The fluorescence decay of Bs-PFK appears to represent two ground-state species with populations of 40% for the shorter lifetime component and 60% for the longer lifetime component. Amplitudes of fluorescence decays equal ground-state populations when the absorption and emission spectra

and radiatives rates of the species are the same. In Bs-PFK the two lifetime components have the same emission spectra and probably similar if not identical absorption spectra and radiative rates. The equilibrium between the two states does not shift in the temperature range studied. The arguments for two ground-state conformations of Bs-PFK follow. First, analysis of time-resolved fluorescence data according to various models supports two discrete decay components with positive amplitudes. There is no hint of excited-state reactions such as dipolar (solvent) relaxation in the decay-associated spectra, in the form of either negative amplitude or red-shifted emission of the long lifetime component. Second, the two lifetime components are quenched at different rates by acrylamide: 4×10^8 M^{-1} s^{-1} for the 1.6-ns component and 1.4×10^8 M^{-1} s^{-1} for the 4.5-ns component. Differential acrylamide quenching of two lifetime components was also observed for the single tryptophan in RNase T1 at pH 7.4, with quenching rates of 9×10^8 M^{-1} s^{-1} for the 1.6-ns component and 1.5×10^8 M^{-1} s^{-1} for the predominant 3.9-ns component (44). The association of different bimolecular quenching rates with different lifetimes of single tryptophan residues is taken as evidence of distinguishable protein conformations (44–46). Third, the indole ring in Bs-PFK is relatively immobile. Mobility of the tryptophan side chain often (11, 33), though not always (47), produces a distribution of lifetimes. Both the high steady-state anisotropy $\langle r \rangle = 0.175 \pm 0.003$ at 25°C and relatively high initial anisotropy $r(0) = 0.19$ are consistent with a rigid tryptophan having little internal motion. The lower $r(0)$ in Bs-PFK compared to the limiting value for tryptophan at the same excitation wavelength may be due to differences in polarity of the medium, which would shift the relative energies of the ^1L_a and ^1L_b excited states (48) in a region where the polarization is changing rapidly (43). Alternatively, the usual explanation of rapid librational motion may obtain. We failed to resolve a second anisotropy decay component with short rotational correlation time, so the motion would have to be faster than the time resolution of our experiments.

Bs-PFK has one tryptophan at position 179 in the polypeptide chain, but the enzyme is a tetramer with four tryptophans/molecule. The subunit structure introduces additional opportunities for ground-state heterogeneity, such as association-dissociation reactions, allosteric forms, and non-identical subunit conformations. Mammalian PFK undergoes reversible self-association as a function of solution variables (49). The two decay components of Bs-PFK do not represent different oligomeric species as judged by static and dynamic light scattering and time-resolved emission anisotropy. The molecular weight, hydrodynamic radius, and hydrodynamic volume concur that the tetramer is the only species present in significant amounts. Static light scattering is not highly sensitive to the presence of monomer or dimer amid excess tetramer. Dynamic light scattering has greater potential for resolving heterogeneous mixtures, yet there was no sign of smaller particles at the level of precision possible with such dilute solutions. The rotational correlation time is even more sensitive to size, and here too there was no ev-

idence of heterogeneity in the anisotropy decay. Furthermore, the hydrodynamic radii determined from translational and rotational diffusion measurements agree reasonably well: $R_h = 40$ Å from dynamic light scattering and $R_h = (3V_h/4\pi)^{1/3} = 36$ Å from anisotropy decay, considering the experimental limitations. A hydrodynamic radius of 36–40 Å is larger then the 34-Å radius estimated without hydration. The discrepancy can be reconciled by considering the hydration layer. Finally, the oligomeric structure of Bs-PFK does not depend on solution variables such as pH, despite large variation in enzymatic activity in the region pH 6 to 9 (50).

The tryptophan fluorescence of Bs-PFK is almost completely insensitive to the allosteric transition from active R to inactive T state. The only perceptible changes are a slight red shift in emission maximum and small drop in quantum yield in the T-state conformation. The fluorescence decays of both allosteric forms are biexponential with the same lifetimes and relative amplitudes. Comparison of the R and T structures of Bs-PFK shows that the quaternary change involves a 7° rotation of rigid dimers with no significant change at the large interface (5). W179 is in helix 7 in the inner layer of α helices, in the midst of an extensive hydrophobic contact between the two subunits of the dimer. Fig. 8 illustrates the distances to various functional groups within 8 Å of the indole ring in the R structure. The three waters are absent in the T structure. Most of the other functional groups are in the same place. The F759 peptide nitrogen and carbonyl and the V762 peptide nitrogen move at least 0.1–0.2 Å further away in the T state. The fluorescence results concur that the allosteric transition does not perturb the monomer subunit interface.
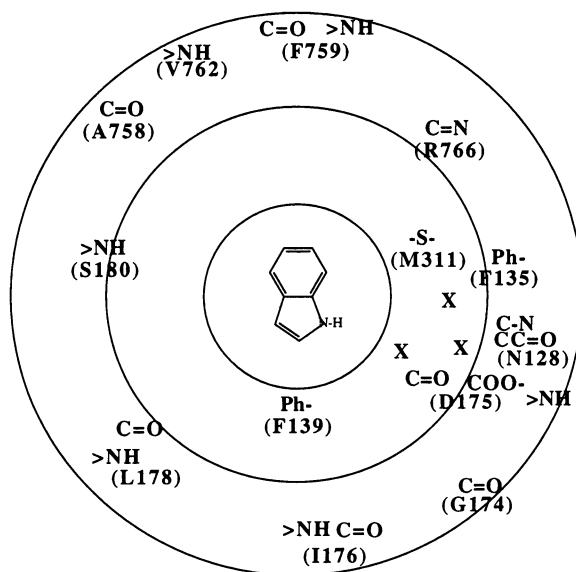

FIGURE 8   Functional groups within 8 Å of W179 in R structure of Bs-PFK. Circles denote 4-, 6-, and 8-Å distances from the center of the indole ring (*C8-C9 bond*). (*>NH*) peptide nitrogen, (*C=O*) peptide carbonyl, (*C-N*) amide nitrogen, (*CC=O*) amide carbonyl, (*C=N*) guanidinium, (*Ph-*) phenyl, (*COO-*) carboxylate, (*-S-*) sulfur.

Although the subunits are chemically identical and the tetramer generally has 222 symmetry, small differences between subunits occur in some of the crystal structures of PFK. These are most discernible in the two R-state structures of Ec-PFK (3, 4), but they are also apparent in the T-state structure of Bs-PFK (5). The most intriguing differences from a functional standpoint are the "closed" and "open" subunit structures of Ec-PFK complexed with its reaction products, which probably represent two intermediates in catalysis (3). There is some suggestion in the electron density map for the R-state structure of Bs-PFK of a similar motion in the active site. Also potentially significant are the minor variations between subunits in the conformation of the allosteric loop in the T structure of Bs-PFK (5, 51). In the 8-Å region around indole, the positions of the N128 amide nitrogen and carbonyl, F135 and F139 phenyl rings, D175 carboxylate and peptide carbonyl, M311 sulfur, A778 peptide carbonyl, and I176 and F259 peptide nitrogens and carbonyls differ by 0.2–0.7 Å among subunits. It is not known whether differences in subunit conformation occur in solution, but their presence would have implications for the fluorescence decay kinetics. If the tryptophan environments are identical, then energy transfer between subunits is without effect. Energy transfer between tryptophans in different environments would be indistinguishable from ground-state heterogeneity if their emission spectra were the same. However, the relative amplitudes and decay times would depend on the energy transfer rates.

The crystal structure shows that W179 is buried in the large interface. In the monomer the indole ring lies in a hydrophobic pocket with half of the benzene ring protruding on the surface. The benzene ring is capped by hydrophobic residues on the other subunit in the dimer. The radiative rate of indole derivatives is higher in nonpolar solvents than in water (29). The relatively high radiative rate of W179 and somewhat blue emission maximum are consistent with a hydrophobic environment in the protein. The weak temperature dependence of the fluorescence quantum yield and lifetime as well as the absence of a deuterium isotope effect indicate that the tryptophan is not accessible to bulk aqueous solvent. Isotopically sensitive solvent quenching is the major temperature-dependent nonradiative decay process in aqueous indoles (16). It is characterized by high frequency factors and activation energies, on the order of 10^{15}–10^{17} s^{-1} and 11–13 kcal/mol, respectively, in water. There is no evidence for water quenching of Bs-PFK fluorescence. In addition, the very low quenching rate constant for iodide, near the limits of detection in steady-state experiments, implies that W179 is inaccessible to small solute molecules. Iodide quenches via the heavy atom effect on intersystem crossing, which requires close contact (52). The moderate quenching by acrylamide likely involves a through-space mechanism, such as electron transfer or exchange (53). The solute quenching parameters of the partially buried tryptophan in RNase T1 are similar to Bs-PFK (30, 44). Acrylamide quenching of RNase T1 was proposed to occur via electron transfer over distances of 1.8 to 3 Å (44). In Bs-PFK the tryptophan is buried deeper

in the protein. W179 is about 11 Å from the outer surface and 13 Å from the solvent-filled hole through the center of the tetramer (54). Rotation about the C^α-C^β bond only appears to bring the indole ring a few Å closer to either protein surface. These distances seem rather far for efficient electron transfer or exchange, both of which drop off exponentially with distance. Dipole-dipole energy transfer operates over longer distances. The Forster critical distance R_o for energy transfer from Bs-PFK tryptophan donor to acrylamide acceptor is 7 Å.

In summary, the evidence presented in this paper demonstrates that the heterogeneous fluorescence decay of Bs-PFK is not due to multiple oligomeric species, R- and T-state allosteric forms, or excited-state reactions such as dipolar relaxation. It also argues convincingly for two discrete microconformational states of the single tryptophan, with different acrylamide quenching rates. These may reflect different subunit conformations in the tetramer that are important in enzyme function or random local fluctuations in the tryptophan environment. Whatever their origin, the lifetime differences between microstates must be due to differences in the proximity of protein functional groups that quench tryptophan fluorescence. The biexponential fluorescence decay is not significantly affected by structural differences in the R- and T states, so the internal waters probably have no role in quenching. Several functional groups in the 8-Å radius around W179 have been proposed to quench indole fluorescence by excited-state proton or electron transfer reactions, including arginine, aspartic acid, asparagine, and methionine side chains as well as the peptide carbonyl (12, 33, 55–57). Present knowledge is insufficient to specify the quenching groups in Bs-PFK. Rotation of the tryptophan side chain would put the indole ring <4 Å from the I176, D175, and G174 peptide carbonyls and change the proximities of the R766 guanidinium, D175 carboxylate, N128 amide nitrogen and carbonyl, and M311 sulfur. Distinct conformational states of Bs-PFK could conceivably be rotamers of W179 that do not interconvert on the fluorescence time scale. Likewise, slow motions of the protein matrix which move quenching functional groups relative to W179 might also produce the ground-state heterogeneity.

REFERENCES

1. Goldhammer, A. R., and H. H. Paradies. 1979. Phosphofructokinase: structure and function. In Current Topics in Cellular Regulation. B. L. Horecker and E. R. Stadtman, editors. Academic Press, New York. pp. 109–141.

2. Valdez, B. C., B. A. French, E. S. Younathan, and S. H. Chang. 1989. Site-directed mutagenesis in Bacillus stearothermophilus fructose-6-phosphate 1-kinase. J. Biol. Chem. 264:131–135.

3. Shirakihara, Y., and P. R. Evans. 1988. Crystal structure of the complex of phosphofructokinase from *Escherichia coli* with its reaction products. *J. Mol. Biol.* 204:973–994.

4. Rypniewski, W. R., and P. R. Evans. 1989. Crystal structure of unliganded phosphofructokinase from *Escherichia coli. J. Mol. Biol.* 207:805–821.

5. Schirmer, T., and P. R. Evans. 1990. Structural basis of the allosteric behaviour of phosphofructokinase. *Nature (Lond.)* 343:140–145.

6. Kolb, E., P. J. Hudson, and J. I. Harris. 1980. Phosphofructokinase: complete amino-acid sequence of the enzyme from *Bacillus stearothermophilus. Eur. J. Biochem.* 108:587–597.

7. Hellinga, H. W., and P. R. Evans. 1985. Nucleotide sequence and high-level expression of the major *Escherichia coli* phosphofructokinase. *Eur. J. Biochem.* 149:363–373.

8. French, B. A., and S. H. Chang. 1987. Nucleotide sequence of the phosphofructokinase gene from *Bacillus stearothermophilus* and comparison with the homologous *Escherichia coli* gene. *Gene (Amst.)* 54:65–71.

9. Eftink, M. R. 1991. Fluorescence techniques for studying protein structure. *In* Methods of Biochemical Analysis. C. H. Suelter, editor. Wiley, New York. pp. 127–205.

10. Royer, C. A., J. A. Gardner, J. M. Beechem, J.-C. Brochon, and K. S. Matthews. 1990. Resolution of the fluorescence decay of the two tryptophan residues of *lac* repressor using single tryptophan mutants. *Biophys. J.* 58:363–378.

11. Alcala, J. R., E. Gratton, and F. G. Prendergast. 1987. Interpretation of fluorescence decays in proteins using continuous lifetime distributions. *Biophys. J.* 51:925–936.

12. Yu, H.-T., W. J. Colucci, M. L. McLaughlin, and M. D. Barkley. 1992. Fluorescence quenching in indoles by excited-state proton transfer. *J. Am. Chem. Soc.* 114:8449–8454.

13. Petrich, J. W., J. W. Longworth, and G. R. Fleming. 1987. Internal motion and electron transfer in proteins: a picosecond fluorescence study of three homologous azurins. *Biochemistry.* 26:2711–2722.

14. Hansen, J. E., J. W. Longworth, and G. R. Fleming. 1990. Photophysics of metalloazurins. *Biochemistry.* 29:7329–7338.

15. Lakowicz, J. R., and H. Cherek. 1980. Dipolar relaxation in proteins on the nanosecond timescale observed by wavelength-resolved phase fluorometry of tryptophan fluorescence. *J. Biol. Chem.* 255:831–834.

16. McMahon, L. P., W. J. Colucci, M. L. McLaughlin, and M. D. Barkley. 1992. Deuterium isotope effects in constrained tryptophan derivatives: implications for tryptophan photophysics. *J. Am. Chem. Soc.* 114:8442–8448.

17. Kotlarz, D., and H. Buc. 1982. Phosphofructokinases from *Escherichia coli. Methods Enzymol.* 90:60–70.

18. French, B. A., B. C. Valdez, E. S. Younathan, and S. H. Chang. 1987. High-level expression of *Bacillus stearothermophilus* 6-phosphofructo-1-kinase in *Escherichia coli. Gene (Amst.)* 59:279–283.

19. Chen, R. F. 1967. Fluorescence quantum yields of tryptophan and tyrosine. *Anal. Lett.* 1:35–42.

20. Kirby, E. P., and R. F. Steiner. 1970. The influence of solvent and temperature upon the fluorescence of indole derivatives. *J. Phys. Chem.* 74:4480–4490.

21. Petrich, J. W., M. C. Chang, D. B. McDonald, and G. R. Fleming. 1983. On the origin of nonexponential fluorescence decay in tryptophan and its derivatives. *J. Am. Chem. Soc.* 105:3824–3832.

22. Beechem, J. M. 1989. A second generation global analysis program for the recovery of complex inhomogeneous fluorescence decay kinetics. *Chem. Phys. Lipids.* 50:237–251.

23. Kolber, Z. S., and M. D. Barkley. 1986. Comparison of approaches to the instrumental response function in fluorescence decay measurements. *Anal. Biochem.* 152:6–21.

24. Russo, P. S., M. J. Saunders, K. H. Langley, S. Kuehl, and L. M. DeLong. 1986. Zero-angle depolarized light scattering of a colloidal polymer. *Anal. Chim. Acta.* 189:69–87.

25. Leite, R. C. C., R. S. Moore, S. P. S. Porto, and J. E. Ripper. 1965. Angular dependence of the Rayleigh scattering from low-turbidity molecular liquids. *Phys. Rev. Lett.* 14:7–9.

26. Berne, B. J., and R. Pecora. 1976. Dynamic Light Scattering. Wiley, New York. 376 pp.

27. Russo, P. S., K. H. Langley, and F. E. Karasz. 1984. Dynamic light scattering study of semidilute solutions of a stiff-chain polymer. *J. Chem. Phys.* 80:5312–5325.

28. Koppel, D. E. 1972. Analysis of macromolecular polydispersity in intensity correlation spectroscopy: the method of cumulants. *J. Chem. Phys.* 57:4814–4820.

29. Privat, J.-P., P. Wahl, and J.-C. Auchet. 1979. Rates of deactivation processes of indole derivatives in water-organic solvent mixtures—application to tryptophyl fluorescence of proteins. *Biophys. Chem.* 9:223–233.

30. James, D. R., D. R. Demmer, R. P. Steer, and R. E. Verrall. 1985. Fluorescence lifetime quenching and anisotropy studies of ribonuclease T1. *Biochemistry.* 24:5517–5526.

31. Szabo, A. G., and D. M. Rayner. 1980. Fluorescence decay of tryptophan conformers in aqueous solution. *J. Am. Chem. Soc.* 102:554–563.

32. Hutnik, C. M. L., J. P. MacManus, and A. G. Szabo. 1990. A calcium-specific conformational response of parvalbumin. *Biochemistry.* 29:7318–7328.

33. Harris, D. L., and B. S. Hudson. 1990. Photophysics of tryptophan in bacteriophage T4 lysozymes. *Biochemistry.* 29:5276–5285.

34. Boens, N., L. D. Janssens, and F. C. De Schryver. 1989. Simultaneous analysis of single-photon timing data for the one-step determination of activation energies, frequency factors and quenching rate constants. *Biophys. Chem.* 33:77–90.

35. Ricci, R. W. 1970. Deuterium-isotope effect on the fluorescence yields and lifetimes of indole derivatives—including tryptophan and tryptamine. *Photochem. Photobiol.* 12:67–75.

36. Eftink, M. R., and C. A. Ghiron. 1981. Fluorescence quenching studies with proteins. *Anal. Biochem.* 114:199–227.

37. Huglin, M. B. 1972. Specific refractive index increments. *In* Light Scattering from Polymeric Solutions. M. B. Huglin, editor. Academic Press, New York. pp. 165–331.

38. Ford, N. C. 1983. Theory and practice of correlation spectroscopy. *In* Measurement of Suspended Particles by Quasielastic Light Scattering. B. E. Dahneke, editor. Wiley, New York. pp. 31–78.

39. Paradies, H. H., W. Vetterman, and G. Werz. 1977. Shape of phosphofructokinase from *Escherichia coli* in solution. *Protoplasma.* 92:43–56.

40. Cantor, C. R., and P. R. Schimmel. 1980. Biophysical Chemistry Part II: Techniques for the Study of Biological Structure and Function. Freeman, New York. 846 pp.

41. Sun, M., and P.-S. Song. 1977. Solvent effects on the fluorescent states of indole derivatives—dipole moments. *Photochem. Photobiol.* 25:3–9.

42. Lakowicz, J. R., B. P. Maliwal, H. Cherek, and A. Balter. 1983. Rotational freedom of tryptophan residues in proteins and peptides. *Biochemistry.* 22:1741–1752.

43. Valeur, B., and G. Weber. 1977. Resolution of the fluorescence excitation spectrum of indole into the L_a and L_b excitation bands. *Photochem. Photobiol.* 25:441–444.

44. Chen, L. X.-Q., J. W. Longworth, and G. R. Fleming. 1987. Picosecond time-resolved fluorescence of ribonuclease T1. *Biophys. J.* 51:865–873.

45. Stayton, P. S., and S. G. Sligar. 1991. Structural microheterogeneity of a tryptophan residue required for efficient biological electron transfer between putidaredoxin and cytochrome P-450$_{cam}$. *Biochemistry.* 30:1845–1851.

46. Atkins, W. M., P. S. Stayton, and J. J. Villafranca. 1991. Time-resolved fluorescence studies of genetically engineered *Escherichia coli* glutamine synthetase. Effects of ATP on the tryptophan-57 Loop. *Biochemistry* 30:3406–3416.

47. Vincent, M., J.-C. Brochon, F. Merola, W. Jordi, and J. Gallay. 1988. Nanosecond dynamics of horse heart apocytochrome *c* in aqueous solution as studied by time-resolved fluorescence of the single tryptophan residue (Trp-59). *Biochemistry.* 27:8752–8761.

48. Lami, H., and N. Glasser. 1986. Indole's solvatochromism revisited. *J. Chem. Phys.* 84:597–604.

49. Luther, M. A., G.-Z. Cai, and J. C. Lee. 1986. Thermodynamics of dimer and tetramer formations in rabbit muscle phosphofructokinase. *Biochemistry.* 25:7931–7937.

50. Deville-Bonne, D., F. Bourgain, and J.-R. Garel. 1991. pH dependence

of the kinetic properties of allosteric phosphofructokinase from *Escherichia coli. Biochemistry.* 30:5750–5754.

51. Kundrot, C. E., and P. R. Evans. 1991. Designing an allosterically locked phosphofructokinase. *Biochemistry.* 30:1478–1484.

52. Kasha, M. 1952. Collisional perturbation of spin-orbital coupling and the mechanism of fluorescence quenching. A visual demonstration of the perturbation. *J. Chem. Phys.* 20:71–74.

53. Calhoun, D. B., S. W. Englander, W. W. Wright, and J. M. Vanderkooi. 1988. Quenching of room temperature protein phosphorescence by added small molecules. *Biochemistry.* 27:8466–8474.

54. Evans, P. R., and P. J. Hudson. 1979. Structure and control of phosphofructokinase from *Bacillus stearothermophilus. Nature.* 279:500–504.

55. Steiner, R. F., and E. P. Kirby. 1969. The interaction of the ground and excited states of indole derivatives with electron scavengers. *J. Phys. Chem.* 73:4130–4135.

56. Cowgill, R. W. 1970. Fluorescence and protein structure XVII. On the mechanism of peptide quenching. *Biochim. Biophys. Acta.* 200:18–25.

57. Werner, T. C., and L. S. Forster. 1978. The fluorescence of tryptophyl peptides. *Photochem. Photobiol.* 29:905–914.